Supporting information

Zr Incorporation into TiO_2 Electrodes Reduces Hysteresis and Improves Performance in Hybrid Perovskite Solar Cells while Increasing Carrier Lifetimes

Hirokazu Nagaoka, Fei Ma, Dane W. deQuilettes, Sarah M. Vorpahl, Micah S. Glaz, Adam E. Colbert, Mark E. Ziffer and David S. Ginger*

Department of Chemistry, University of Washington, Box 351700, Seattle, Washington 98195-1700, United States

Corresponding Author e-mail address: ginger@chem.washington.edu.

Experimental methods:

J-V characteristics and time-dependent photocurrent measurements. Current density–voltage (J-V) curves were measured using a source meter (Keithley, 2400 Series) under AM 1.5 G light illumination from a solar simulator (Solar Light Co. model 16S-300) with intensity calibrated to 100 mW/cm^2 using a Si reference cell. The solar cells were masked with a metal aperture to define the active area, typically 0.013 cm^{-2}, and measured in a light-tight sample holder to minimize edge effects. Scanning rates of 0.15V/s or 0.025V/s were used to assess the hysteretic behavior of devices.

External quantum efficiency. Solar cells were illuminated with a monochromated (Acton 2150) 100 W tungsten-halogen light source (Oriel). Photocurrent spectra were measured using a Keithley 2400 source meter. A calibrated silicon photodiode (OSI optoelectronics) was used to

calculate external quantum efficiencies. All photovoltaic measurements were collected with devices under dynamic vacuum (~20 mTorr).

Cyclic voltammetry (CV). Cyclic voltammograms were acquired using a potentiostat (Autolab). Zr-TiO_2 and undoped TiO_2 films cast on FTO served as the working electrodes. The counter electrode and reference electrode were a platinum wire and Ag/AgCl in saturated 3M KCl solution, respectively. Tetrabutylammonium hexaflurophosphate (0.1 M) in anhydrous acetonitrile was used as the supporting electrolyte. Voltammograms were obtained using a scan rate of 0.25 V/s and by sweeping the voltage from 0 V → −1.5 V → 0 V. A ferrocene/ferricinum redox was used as the standard reference (−4.80 V relative to vacuum).[1]

X-ray photoemission spectroscopy (XPS). Zr-TiO_2 and TiO_2 films on FTO were measured in a Kratos Axis Ultra DLD under ultrahigh vacuum. A monochromated Al K-alpha x-ray anode ($h\nu$ = 1486.6 eV) was used to irradiate all samples. Data was collected and analyzed from a 300 x 700 μm spot size. For high-resolution XPS scans, all XPS spectra were taken on a Surface Science Instruments S-probe spectrometer which has a monochromated Al-K-alpha X-ray radiation source under high vacuum (less than 5 x 10^{-9} Torr). X-ray spot size for these acquisitions was approximately 800 μm. The binding energy scales were calibrated by assigning the lowest binding energy C1s peak a binding energy of 285.0 eV.

Scanning Kelvin probe microscopy (SKPM). The surface potential of Zr-TiO_2 and TiO_2 films on FTO were measured using Scanning Kelvin Probe Microscopy (Cypher/AFM, Asylum Research). A Cr/Pt coated tip (300kHz, spring constant 40 N/m) was used for all measurements. Relative work functions were acquired by comparing the average surface potential of Zr-TiO_2 to TiO_2.

Scanning electron microscopy (SEM). Surface and cross-section scanning electron microscopy (SEM) images were collected with an FEI Sirion system at the NanoTech User Facility (NTUF) at the Center for Nanotechnology University of Washington (UW). Top view images were taken of perovskite films deposited and grown on TiO_2 and Zr-TiO_2 electrodes. Cross-section images were conducted on cleaved devices.

UV-VIS measurements. Absorbance spectra of Zr-TiO_2 and TiO_2 films on FTO were acquired on a Agilent 8453 diode array spectrometer.

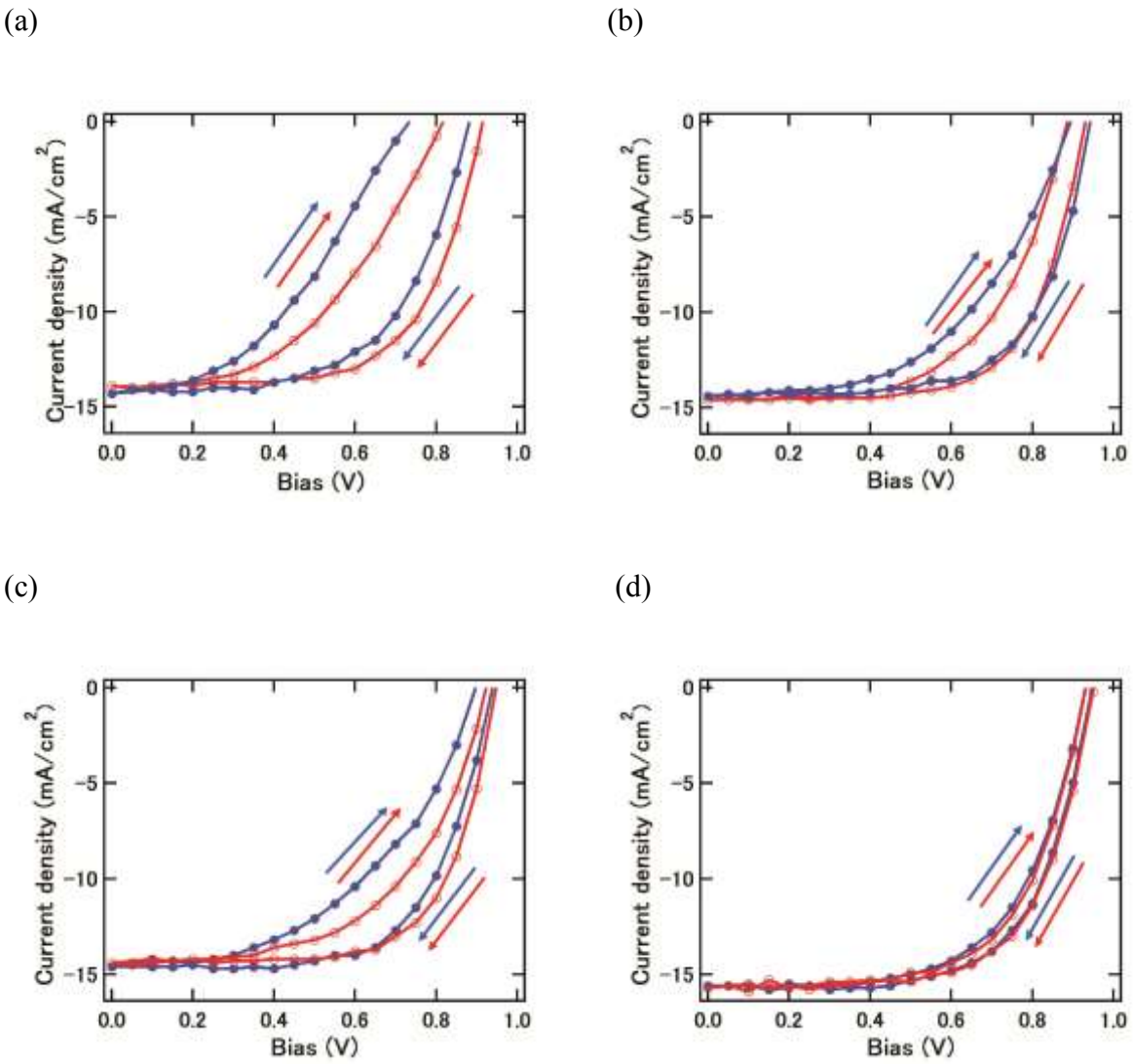

Figure S1 J-V curves of devices with (a) TiO_2 electrodes, (b) Zr-TiO_2 electrodes, (c) TiO_2/pyridine treatment, and (d) Zr-TiO_2/pyridine treatment acquired at the scanning rate of 0.15 V/s (blue filled circle) and 0.025 V/s (red empty circle).

Figure S1 shows the J-V characteristics measured when scanning from open circuit (V_{OC}) to short circuit (SC) and SC to Voc for TiO_2, Zr-TiO_2, TiO_2/pyridine treated, and Zr-TiO_2/pyridine treated devices. We report a significant reduction in the measured hysteresis in pyridine treated devices with Zr-TiO_2 electrodes. This observation is consistent even when

measuring the solar cell with a different scan rate. Devices with TiO_2 electrodes, Zr-TiO_2 electrodes and TiO_2/pyridine treatment show large hysteretic behavior at both scanning rates. To quantify the hysteresis effects, we calculate the hysteresis index (HI) using two different equations that have been proposed in the literature for quantifying hysteresis:[2, 3]

$$\text{Hysteresis index} = \frac{J_{\text{RS}}(0.8\text{V}_{\text{oc}}) - J_{\text{FS}}(0.8\text{V}_{\text{oc}})}{J_{\text{RS}}(0.8\text{V}_{\text{oc}})} \quad (1)$$

where J_{RS} $(0.8V_{OC})$ and J_{FS} $(0.8V_{OC})$ show photocurrent density at 80% of V_{OC} for reverse scan (RS) and forward scan (FS), respectively. Forward and reverse scan mean scanning from Voc to Jsc and scanning from Jsc and Voc, respectively.

$$\text{Hysteresis index} = \frac{J_{\text{scan}-}(\text{V}_{\text{oc}}/2) - J_{\text{scan}+}(\text{V}_{\text{oc}}/2)}{J_{\text{scan}-}(\text{V}_{\text{oc}}/2)} \quad (2)$$

where J_{scan-} $(V_{OC}/2)$ and J_{scan+} $(V_{OC}/2)$ show photocurrent density at 50% of V_{OC} for scan- (RS) and scan+ (FS), respectively. Table 1 shows hysteresis indices obtained from J-V curves in Figure S1 using two different equations with different scan rates.

Table S1 Summary of hysteresis indices with four different devices

	Equation 1 0.15 V/s	Equation 1 0.025 V/s	Equation 2 0.15 V/s	Equation 2 0.025 V/s
TiO_2	0.51	0.41	0.16	0.10
Zr-TiO_2	0.31	0.17	0.05	0.02
TiO_2/pyridine	0.32	0.22	0.12	0.06
Zr-TiO_2/pyridine	0.07	0.05	0.02	0.01

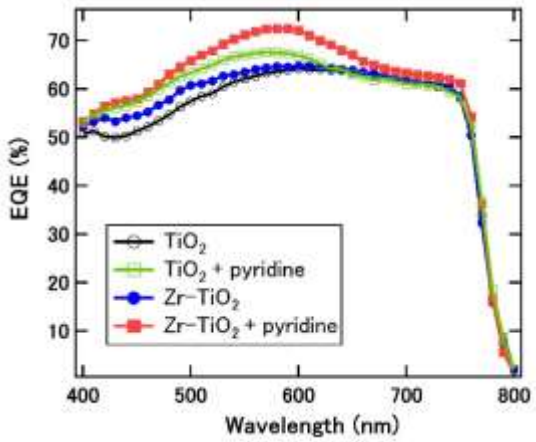

Figure S2 (a) External quantum efficiency spectra of complete devices using Zr-TiO_2 (blue filled circle), TiO_2 (black empty circle), Zr-TiO_2/pyridine treatment (red filled square) and TiO_2/pyridine treatment (green empty square)

Figure S2 shows the external quantum efficiency (EQE) spectra for Zr-TiO_2, TiO_2, Zr-TiO_2/pyridine treated and TiO_2/pyridine treated devices. We find charges are more efficiently extracted in Zr-TiO_2 devices at shorter wavelengths (400 nm to 600 nm) and pyridine treatments improve charge collection efficiency across nearly the entire absorbing spectrum in both Zr-TiO_2 and TiO_2 devices.

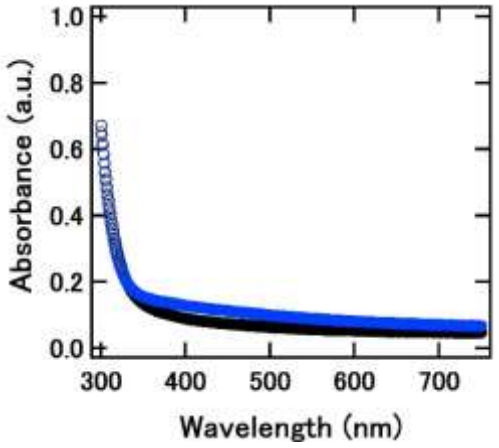

Figure S3 (a) Absorbance spectra of Zr-TiO_2 (blue empty circle) and TiO_2 (black empty circle) films.

(a) (b)

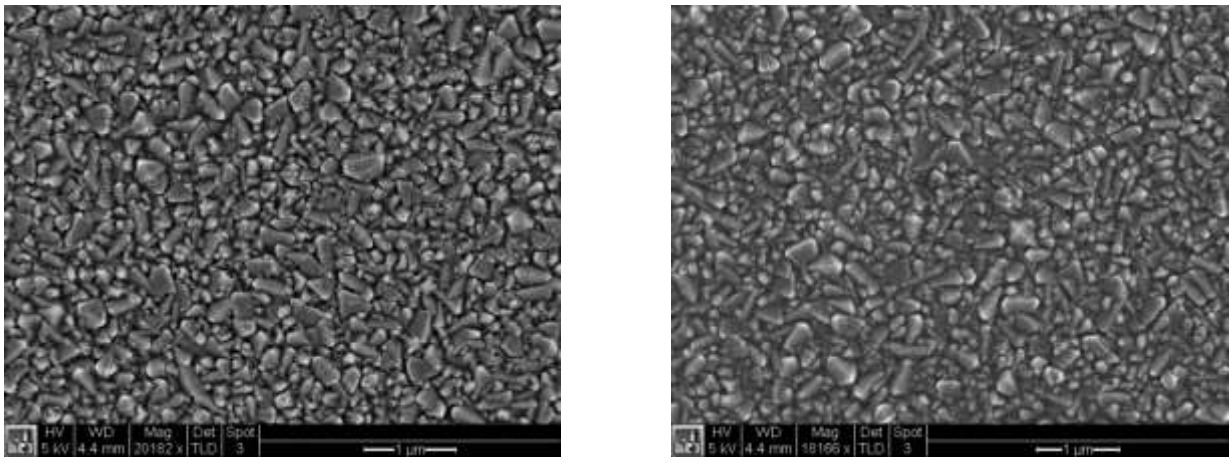

(c) (d)

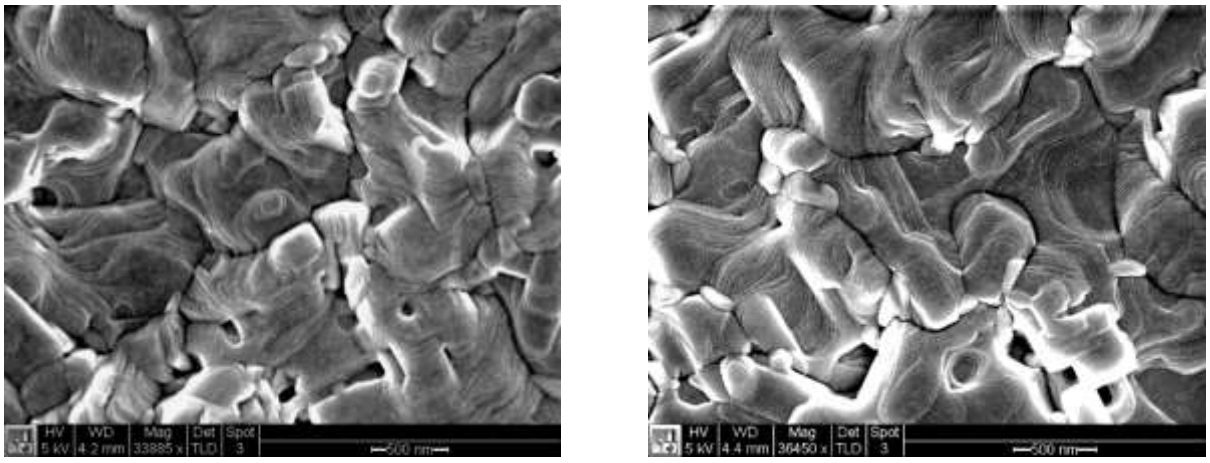

Figure S4 Scanning Electron Microscopy (SEM) images of (a) Zr-TiO_2, (b) TiO_2, (c) perovskite on Zr-TiO_2, (d) perovskite on TiO_2.

(a)

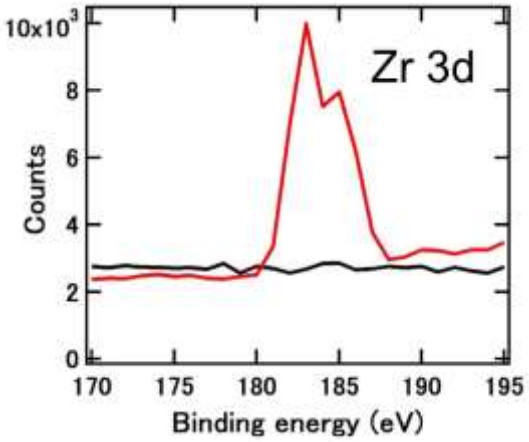

(b)

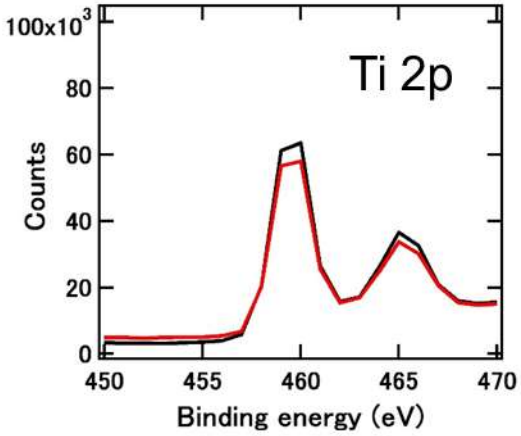

(c)

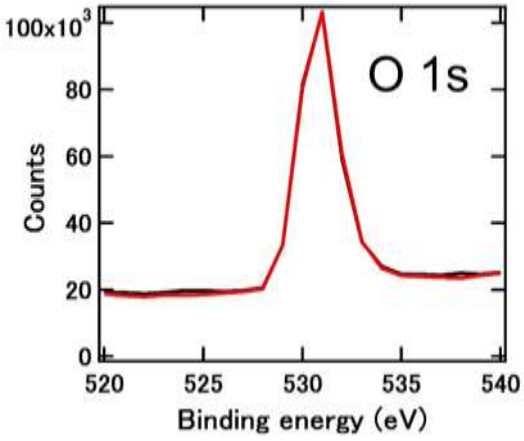

Figure S5 X-ray photoemission spectroscopy (XPS) spectra for Zr-TiO_2 (red) and TiO_2 (black) films on bare FTO. (a) XPS spectra of Zr 3d (b) XPS spectra of Ti 2p (c) XPS spectra of O 1s.

Figure S5 shows X-ray photoemission spectroscopy (XPS) spectra for Zr-TiO_2 and TiO_2 films on FTO. We confirm the successful incorporation of zirconium into TiO_2 by identifying the Zr 3d feature at 182.5 eV[4] and the decrease in intensity of the Ti 2p feature. We also report the Ti 2p and O 1s core level binding energies at 458.5 eV and 530.0 eV, respectively.[4] We integrate Zr

3d and Ti 2p peaks to calculate the Zr and Ti atomic percent in the Zr-TiO_2 film to be ~6% (1 to 15.69).

(a)

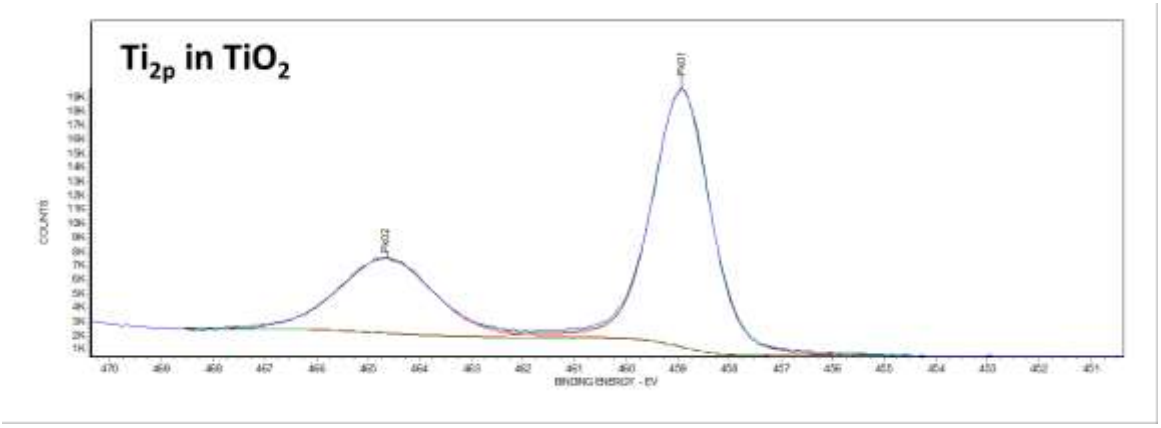

(b)

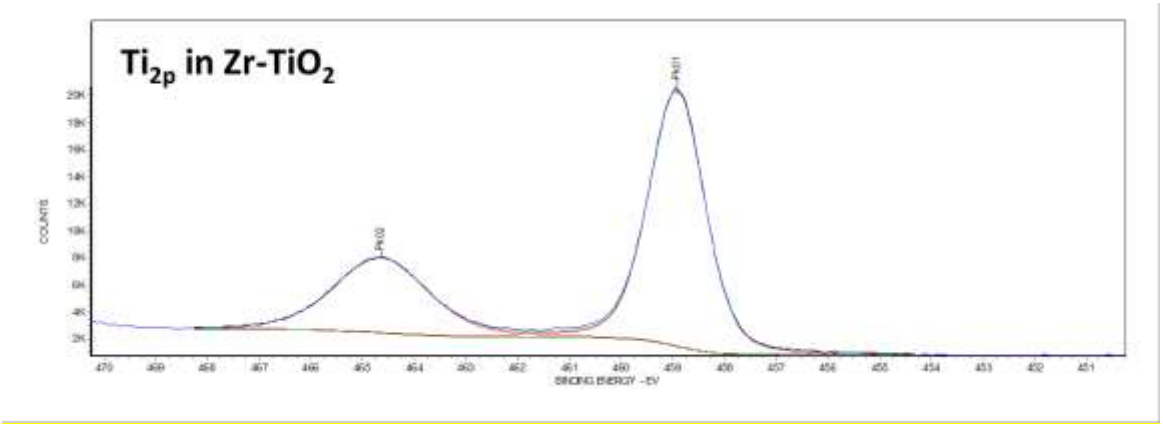

(c)

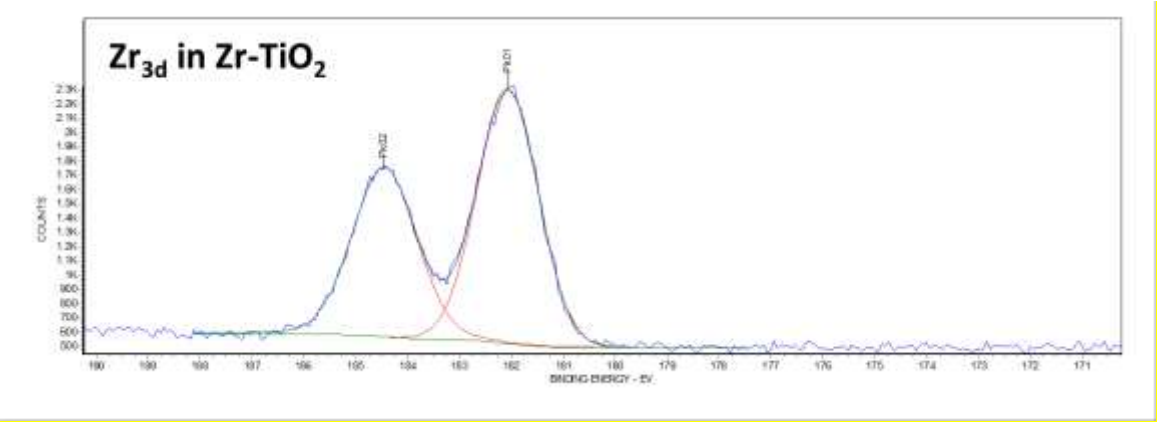

Figure S6 High-resolution XPS spectra of the Ti and Zr regions (a) Ti 2p peak of TiO_2 film (b) Ti 2p peak of Zr-TiO_2 film (c) Zr 3d peak of Zr-TiO_2 film.

Figure S6 and Table S2 show high-resolution XPS scans and peak fit parameters, respectively. Curve fitting of Ti 2p peak in both TiO_2 and Zr-TiO_2 films shows the Ti cation is Ti^{4+}. For Zr 3d peak in Zr-TiO_2 film, the Zr cation is Zr^{4+}.[1, 4, 5]

Table S2 Peak fit parameters

	BE (eV)	FWHM (eV)	Peak
Ti $2p_{3/2}$ (TiO_2)	458.9	1.2	Pk01
Ti $2p_{1/2}$ (TiO_2)	464.6	2.0	Pk02
Ti $2p_{3/2}$ (Zr-TiO_2)	458.9	1.2	Pk01
Ti $2p_{1/2}$ (Zr-TiO_2)	464.6	2.1	Pk02
Zr $3d_{5/2}$ (Zr-TiO_2)	182.1	1.4	Pk01
Zr $3d_{3/2}$ (Zr-TiO_2)	184.4	1.4	Pk02

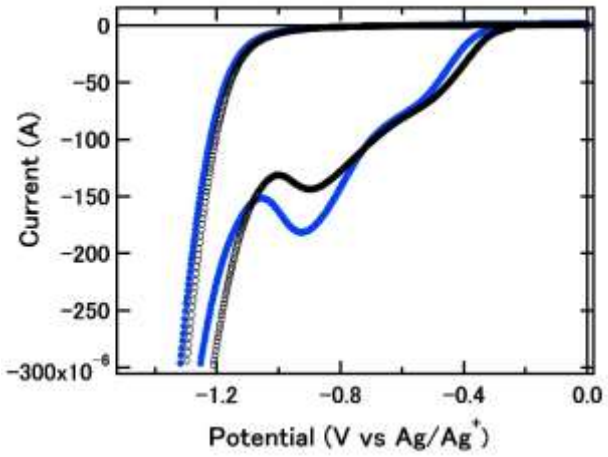

Figure S7 Cyclic voltammetry scans of Zr-TiO_2 (blue filled circle) and TiO_2 (black empty circle) films.

Figure S7 shows the current vs. voltage traces of Zr-TiO_2 (blue) and TiO_2 (black) films on FTO using cyclic voltammetry (CV). We report a slightly higher reduction potential (-0.92 V) for Zr-TiO_2 electrodes, compared to the measured reduction potential for TiO_2 electrodes (-0.87 V). Furthermore, we find an increase in the current amplitude for Zr-TiO_2, suggesting faster reduction kinetics near the CB edge.

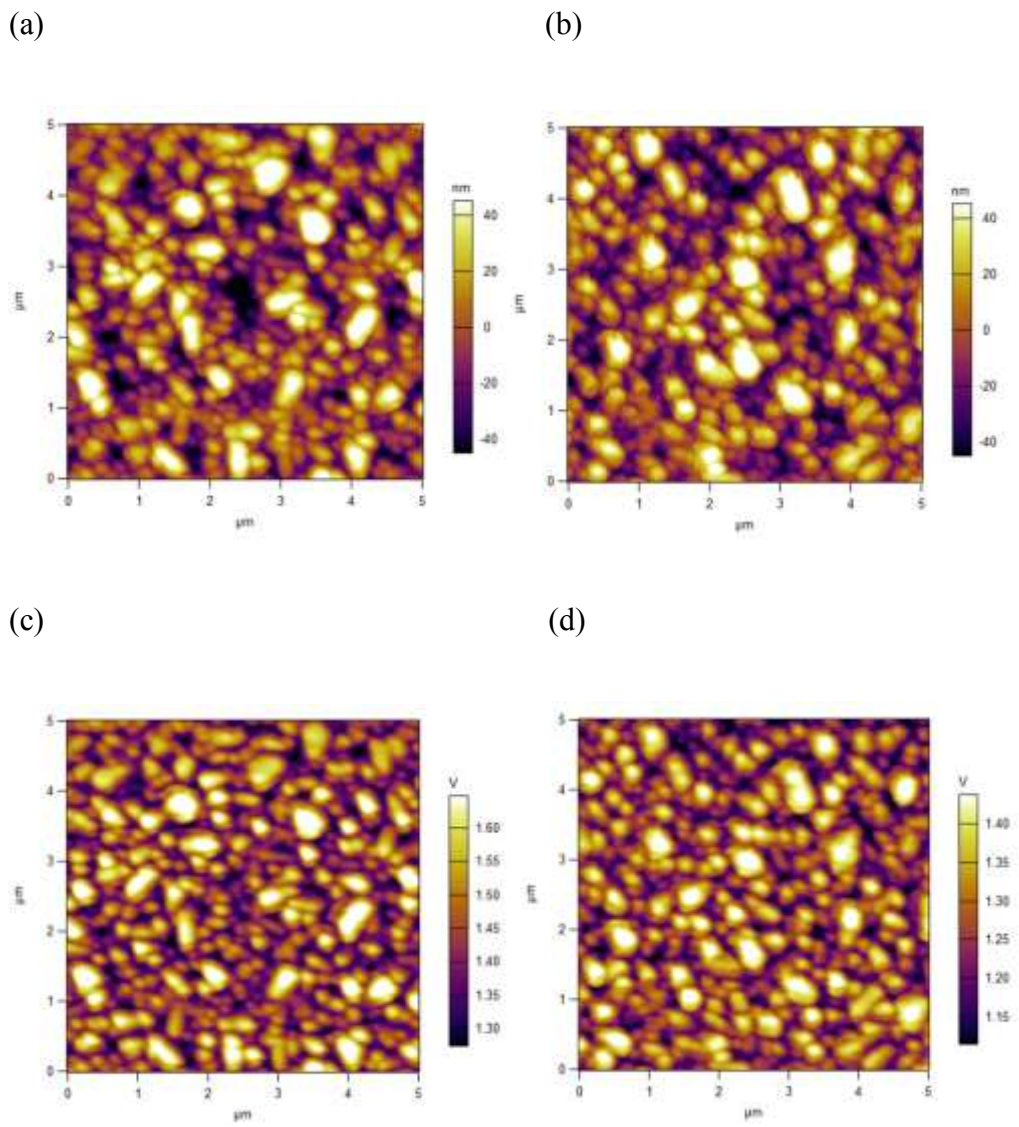

Figure S8 Scanning Kelvin probe microscopy (SKPM) images showing (a, c) topography and surface potential of a Zr-TiO_2 film and (b, d) topography and surface potential of a TiO_2 film.

Figure S8 shows topography and surface potential images obtained using scanning Kelvin probe microscopy (SKPM). The average work function difference between Zr-TiO_2 electrodes and TiO_2 electrodes is 0.18 ± 0.04V, indicating a shallower work function for Zr-TiO_2 electrodes.

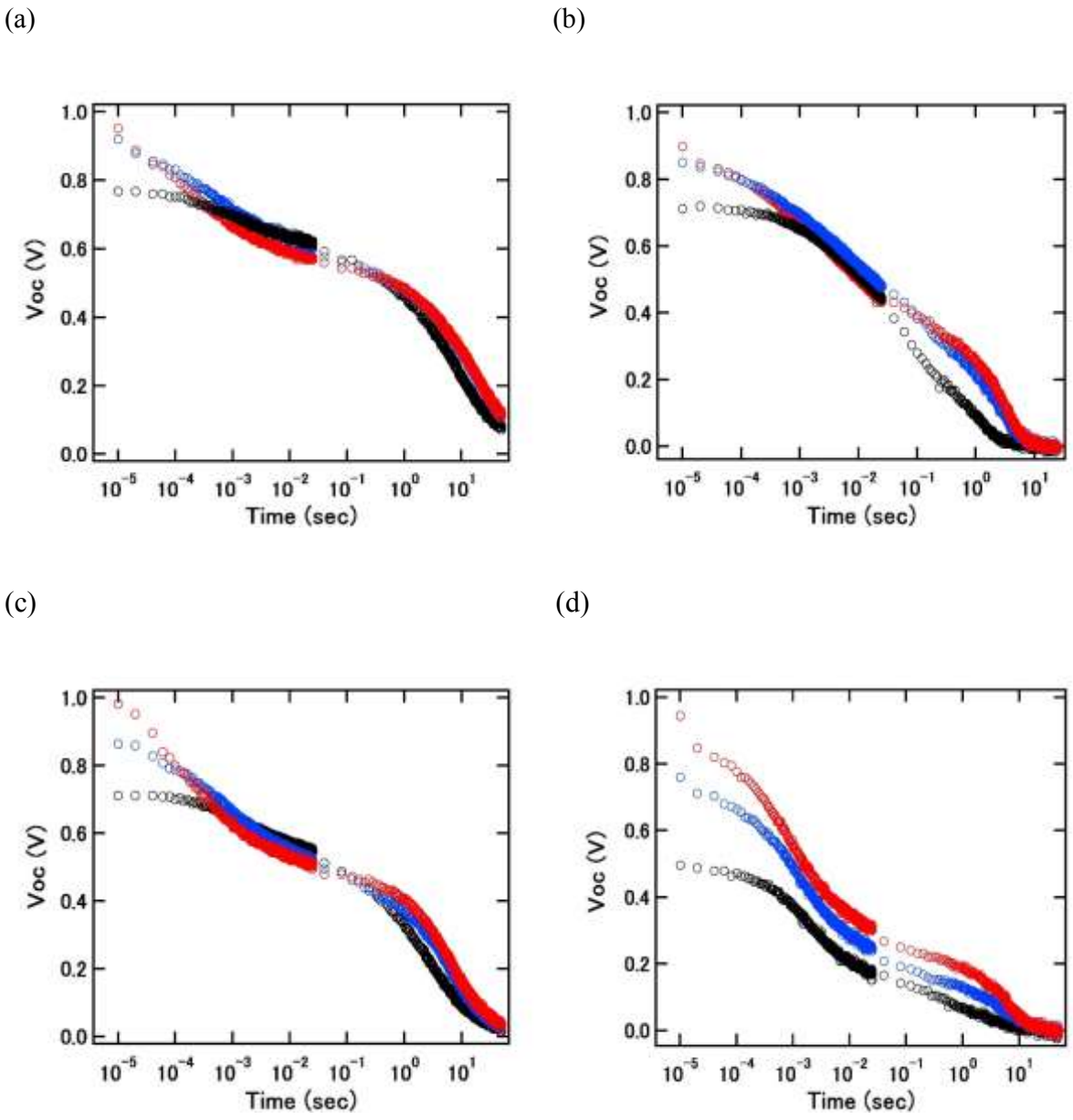

Figure S9 (a) Open circuit voltage transients for the perovskite devices based (a) Zr-TiO_2, (b) TiO_2, (c) Zr-TiO_2/pyridine treatment, (d) TiO_2/pyridine treatment under 118 mW/cm^2 (red circle), 11.1 mW/cm^2 (blue circle) and 2.0 mW/cm^2 (black circle) white LED illuminations.

Figure S9 shows open circuit voltage transients for the four different perovskite devices under three different illumination intensities. Under high illumination intensities, all devices

exhibit a fast photovoltage decay at short time scales ($<10^{-3}$ s) followed by a slower photovoltage decay at longer times ($>10^{-1}$ s).

References

(1) Liu, H.; Tang, J.; Kramer, I.; Debnath, R.; Koleilat, G.; Wang, X.; Fisher, A.; Li, R.; Brzozowski, L.; Levina, L. et al. Electron Acceptor Materials Engineering in Colloidal Quantum Dot Solar Cells. *Adv. Mater.* **2011**, *23*, 3832-3837.

(2) Kim, H.; Park, N. Parameters Affecting I-V Hysteresis of $CH_3NH_3PbI_3$ Perovskite Solar Cells: Effects of Perovskite Crystal Size and Mesoporous TiO_2 Layer. *J. Phys. Chem. Lett.* **2014**, *5*, 2927-2934.

(3) Sanchez, R. S.; Gonzalez-Pedro, V.; Lee, J.-W.; Park, N.-G.; Kang, Y. S.; Mora-Sero, I.; Bisquert, J. Slow Dynamic Processes in Lead Halide Perovskite Solar Cells. Characteristic Times and Hysteresis. *J. Phys. Chem. Lett.* **2014**, *5*, 2357−2363.

(4) Reddy, B.; Chowdhury, B.; Ganesh, I.; Reddy, E.; Rojas, T.; Fernandez, A. Characterization of V_2O_5/TiO_2-ZrO_2 catalysts by XPS and other techniques. *J. Phys. Chem. B* **1998**, *102*, 10176-10182.

(5) Biesingera, M. C.; Lau, L. W. M.; Gersonb, A. R.; Smartb, R. St. C. Resolving surface chemical states in XPS analysis of first row transition metals, oxides and hydroxides: Sc, Ti, V, Cu and Zn. *Appl. Surf. Sci.* **2010**, *257*, 887–898.